Table S1 The most popular geochemical fingerprinting indices used to identify dust provenance in northern China.

Indexes	Regions	References
Eu/Eu*, $(Gd/Yb)_n$, $(La/Yb)_n$, $(La/Sm)_n$	Qilian Mountains	Wei et al. (2017)
Eu/Eu*	Northern China	Chen et al. (2017)
Eu/Eu*, Y/ΣREE, La/Er, La/Gd, Gd/Er, La/Yb, Y/Tb, Y/La, Y/Nd, La/Th	Northern China	Ferrat et al. (2011)
Eu/Eu*, $(La/Yb)_n$, $(La/Sm)_n$, $(Gd/Yb)_n$	Northeastern China	Xie and Chi (2016)
$(La/Yb)_n$	Northern China	Yang et al. (2007)
Eu/Eu*, $(La/Yb)_n$	Chinese Loess Plateau	Jahn et al. (2001)
Eu/Eu*, $(Gd/Yb)_n$, $(La/Sm)_n$	Chinese Loess Plateau	Ding et al. (2001)
Eu/Eu*, $(La/Yb)_n$, La/Th	Chinese Loess Plateau	Gallet et al. (1996)
Th/Sc, La/Th	Chinese Loess Plateau	Liu et al. (1993)

Table S2 Main climate and related conditions at the meteorological station sites in the study region. Their locations are shown in Figure S1. *DP* is the drift potential in vector units and *RDD* is the resultant drift direction; they were calculated using the methods of Fryberger and Dean (1979). U_{mean}, mean annual wind speed; *MAT*, mean annual temperature. High *DP* indicates strong wind erosion in the dust source region and strong transport of dust material to transitional regions (such as the Tengger Desert) and downwind regions (such as the Chinese Loess Plateau).

	Karamay	Hongliuhe	Mazun	Ejina	Hongsan	Zhongwei	Yulin
Elevation (m asl)	500	2692	2200	910	1329	1307	1100
Total annual rainfall (mm)	105	45.5	150	37	70	94	438
MAT (°C)	8.6	11.4	6.3	8.3	9	12	8.1
U_{mean} (m s^{-1})	3.70	4.05	4.19	2.9	3.9	2.6	3.6
DP (VU)	475	268	348	91	405[a]	69[b]	70[c]
RDD (°)	312	76	339	297	317[a]	303[b]	311[c]

[a] Data from Hongsan are from Zhang et al., 2015; [b] Data from Zhongwei are from Dong et al. (2014); [c] Data from Yulin are from Liu and Yang (2018).

Table S3 The composition of trace elements and rare earth elements at the 40 sample sites. Site abbreviations: A, Alxa Plateau; C, Hexi Corridor and its adjacent region; G, Guerbantonggute Desert; H, Heihe River Basin; L, Lanzhou; M, Mu Us Desert; Q, Qaidam Basin; T, Tengger Desert.

		G1	G2	G3	G4	G5	G6	G7	Q1	Q2	Q3	Q4	Q5	A1	A2	A3	A4	A5
Trace elements (μg/g)	Sc	13.7	15.9	14.1	11.7	14.8	16.8	13.4	10.8	11.7	15.4	12.8	16.8	13.8	8.75	16.3	15.8	19
	Rb	112	87.1	126	108	132	121	122	115	83.5	109	71.8	105	135	89.7	93.1	113	103
	Sr	264	261	401	420	286	239	610	271	356	340	90.6	123	304	298	322	314	316
	Y	33.6	49.6	29.8	29.8	29.7	28.7	26.4	27.6	38.5	34.5	31.2	42	26.6	20.1	32	37.2	36.3
	Zr	233	359	179	150	218	164	179	389	315	290	166	223	232	210	316	395	254
	Nb	11	15.4	10.6	9.21	11.4	10.9	9.03	15.4	14.4	15.8	18.9	15.5	12.6	7.32	13.5	17.8	11.5
	Ba	522	375	539	563	493	427	480	539	489	575	3.52	6.43	637	780	600	609	478
	Hf	6.33	10.1	4.81	4	5.77	4.47	4.82	10.4	8.79	8.11	4.78	5.74	6.17	5.31	8.56	10.4	6.8
	Ta	0.892	1.47	0.82	0.771	0.953	0.887	0.716	1.25	1.25	1.29	4.83	4.24	1.08	1.05	1.13	1.76	0.89
	Pb	19.9	20.2	23.5	19.7	22.3	16.9	19	21	13.9	23.7	32.3	5.27	21.4	15.6	19.2	25.7	22.9
	Th	11.2	14.7	11.6	13.1	12.2	10.6	9.67	25.2	11.9	13.6	14.1	25.1	17.1	6.35	8.59	15.7	11.5
Rare earth elements (μg/g)	La	31.6	45	30.5	34.4	35.6	28.4	25	35.5	38.2	39.4	20.2	27.6	34.3	23.9	39.4	18.7	25.9
	Ce	68	97.7	65.5	74.4	78.2	64.8	52	76.5	80.8	83.7	39.2	52.5	73.9	49.1	83.7	37.3	57.6
	Pr	7.98	11.2	7.56	8.65	8.91	7.25	6.22	9.17	9.26	9.66	4.5	6.34	8.79	5.58	9.54	4.46	6.82
	Nd	31.4	44.3	29.9	34.2	34.8	28.9	24.6	35.6	34.9	37.4	17.2	24	34.9	21.5	36.4	17.3	27.6
	Sm	6.36	9.41	6	7.01	7.01	5.95	5.05	6.98	6.55	7.56	3.33	4.85	7.22	4.31	7.01	3.6	5.93
	Eu	1.34	1.68	1.26	1.34	1.35	1.31	1.06	1.17	1.2	1.48	0.66	0.91	1.49	0.94	1.18	0.84	1.31
	Gd	5.83	8.73	5.5	6.02	5.65	5.16	4.44	5.58	5.76	6.51	2.96	4.06	6.39	3.73	5.53	3.23	5.39
	Tb	0.91	1.39	0.84	0.93	0.87	0.82	0.72	0.84	0.96	1.02	0.46	0.64	1.03	0.59	0.84	0.54	0.87
	Dy	5.46	8.19	4.93	5.22	4.96	4.8	4.34	4.8	6.15	5.99	2.73	3.8	6.27	3.45	4.68	3.3	5.28
	Ho	1.14	1.68	1.02	1.02	1.02	0.98	0.91	0.96	1.3	1.21	0.56	0.77	1.26	0.72	0.92	0.7	1.1
	Er	3.24	4.81	2.9	2.81	2.91	2.77	2.59	2.75	3.77	3.4	1.6	2.13	3.58	2.03	2.61	2.05	3.14
	Tm	0.48	0.7	0.41	0.4	0.42	0.4	0.38	0.4	0.55	0.49	0.23	0.31	0.52	0.3	0.37	0.3	0.46

	Yb	3.18	4.85	2.76	2.6	2.87	2.68	2.58	2.81	3.59	3.36	1.55	2.05	3.46	2.01	2.54	2.08	3.14
	Lu	0.48	0.74	0.42	0.39	0.43	0.41	0.39	0.43	0.53	0.51	0.24	0.31	0.52	0.3	0.38	0.32	0.48

		A6	A7	C1	C2	C3	C4	C5	C6	C7	C8	H1	H2	H3	H4	H5	H6	H7
Trace elements (μg/g)	Sc	12.1	11.1	18.7	16.1	12.3	12.2	13.1	14.5	10.9	10.2	16.6	15.4	16.9	15.1	13.3	12.1	11.7
	Rb	102	107	105	97.5	122	83.6	79.7	70.9	94.9	94	100	99.2	165	86.7	118	101	102
	Sr	274	236	307	261	257	246	260	263	234	230	256	257	277	270	344	227	240
	Y	32.7	27.1	36.8	42.8	27.9	28.6	35.1	40.6	20.7	20.3	31.1	37.8	26	42.9	23.7	23.8	30.2
	Zr	369	454	222	206	254	423	642	847	218	199	328	785	120	577	179	204	207
	Nb	13.9	13.7	12.1	10.3	13.4	13.2	15.3	19.4	10.7	9.88	19.7	22.9	12.6	16.2	11.3	12.4	11.5
	Ba	674	596	472	473	523	538	527	432	883	1532	912	642	649	543	640	585	601
	Hf	10.1	12.2	5.64	5.48	6.64	11.1	16.5	22.1	5.49	5.47	8.92	20.9	3.28	15.7	4.65	5.43	5.66
	Ta	1.07	1.13	0.926	0.82	1.19	1.35	1.57	2.11	0.792	0.838	1.5	2.23	0.952	1.44	0.853	1.2	0.887
	Pb	18.3	20.8	22.3	33.9	20.1	17.3	17.5	17.7	43.2	27.7	22.3	21.4	27.2	23.2	23.9	16.6	17.1
	Th	12.5	18.8	10.7	11.9	14.4	11.5	14.3	17	8.7	8.28	28	22.7	14.8	21.6	11.9	10.2	11.3
Rare earth elements (μg/g)	La	48.8	41.8	44.1	32.2	33.4	30.7	32.8	48.1	23.5	29	33.5	34.6	38.9	32.9	50.6	54.2	35
	Ce	107	91.8	91	70.1	73.7	63.9	68.7	101	47.6	57.7	72.6	79.8	85.4	69	107	119	74.2
	Pr	12.3	10.5	10.7	8.47	8.59	7.21	7.66	11.9	5.54	6.5	8	9.37	9.6	7.81	11.6	13	8.37
	Nd	46.7	39.9	41	33.7	34	27	28.6	45	21.3	24.2	30.1	37.1	36	29.4	42.8	48.8	31.8
	Sm	9.03	7.73	8.01	7.09	7.17	5.08	5.43	9	4.15	4.55	5.84	7.66	7.06	5.67	7.8	9.11	6.11
	Eu	1.65	1.44	1.56	1.51	1.49	1.07	1.1	1.6	0.88	0.97	1.19	1.35	1.14	1.14	1.46	1.5	1.09
	Gd	7.5	6.53	6.73	6.37	6.69	4.47	4.75	7.96	3.62	4.01	4.95	5.97	5.76	5.02	6.39	7.49	5.06
	Tb	1.17	1.02	1.06	1.02	1.08	0.68	0.71	1.23	0.56	0.61	0.78	0.91	0.87	0.78	0.97	1.14	0.79
	Dy	6.81	5.94	6.23	6.12	6.84	3.97	4.07	7.18	3.23	3.57	4.49	5.28	4.8	4.69	5.46	6.4	4.47
	Ho	1.41	1.23	1.26	1.25	1.46	0.81	0.81	1.48	0.65	0.73	0.91	1.12	0.96	0.96	1.11	1.31	0.91
	Er	4.05	3.5	3.62	3.58	4.2	2.27	2.29	4.24	1.79	2.07	2.54	3.31	2.69	2.72	3.13	3.75	2.56
	Tm	0.6	0.51	0.53	0.53	0.61	0.32	0.33	0.62	0.26	0.3	0.36	0.51	0.39	0.4	0.45	0.55	0.37

Yb	4.15	3.52	3.59	3.54	4.1	2.17	2.21	4.27	1.68	2.01	2.43	3.52	2.77	2.66	2.99	3.86	2.48
Lu	0.64	0.53	0.55	0.54	0.61	0.33	0.33	0.65	0.25	0.3	0.37	0.55	0.43	0.41	0.46	0.61	0.37

	H8	H9	H10	M	T1	T2	T3	L	K1	K2	K3	K4	K5	K6	K7
Sc	12	12.1	9.18	11	8.75	12.6	11.6	2.29	8.65	8.10	4.35	7.46	6.38	6.61	4.45
Rb	103	106	81.5	83.9	88.8	120	112	25.1	25.16	27.10	30.22	28.79	29.23	32.24	27.4
Sr	256	244	229	232	224	210	262	121	143.58	133.87	125.88	131.57	124.10	161.31	152.32
Y	27.5	24.7	18	26	19.5	26.4	26.3	35.6	20.27	24.55	13.33	12.49	14.07	13.89	11.58
Zr	254	223	124	326	187	234	309	268	132.03	650.10	62.21	73.99	91.22	96.49	116.46
Nb	12.4	11.1	8.84	10.7	9.86	12.3	11.8	15.6	10.98	8.98	5.85	6.55	6.95	6.54	4.96
Ba	631	670	532	449	599	644	627	758	345.89	268.32	236.94	275.71	242.17	220.31	198
Hf	6.83	5.75	3.18	8.66	4.8	5.98	8.18	6.74	4.72	19.59	2.21	2.49	3.03	3.26	3.75
Ta	1.75	0.902	0.664	1.32	0.673	0.965	0.925	4.10	1.21	1.01	0.67	0.77	0.72	0.67	0.52
Pb	62.6	22.6	267	18.6	38	162	103	12.4	17.71	18.70	16.66	16.08	17.08	18.15	21.01
Th	11.6	10.2	7.94	13.2	7.83	11.4	13.1	36.2	25.98	38.59	13.99	16.76	19.87	15.63	18.38
La	28.3	28.4	30.7	33.7	26	38.4	36.7	40.1	32.93	38.41	18.56	24.27	25.59	19.73	18.77
Ce	56.2	62.4	64.3	71	49.2	74.3	70.7	71.9	64.48	75.64	36.39	48.26	49.69	39.11	37.98
Pr	6.38	7.23	7.1	8.21	5.55	8.23	8.01	7.47	7.58	8.61	4.24	5.63	5.74	4.56	4.42
Nd	23.9	27.9	26.9	31.3	20.9	30.7	29.9	28.1	29.42	32.73	16.37	21.78	22.10	17.44	17.16
Sm	4.82	5.56	5.22	6.13	3.88	5.8	5.64	5.48	5.91	6.23	3.34	4.35	4.26	3.51	3.33
Eu	1.06	1.18	1.04	1.19	0.83	1.16	1.08	1.02	0.92	0.93	0.65	0.74	0.73	0.64	0.59
Gd	4.67	4.85	4.62	5.22	3.38	4.98	4.78	4.71	5.49	5.61	3.23	3.75	3.79	3.33	3.15
Tb	0.79	0.75	0.71	0.83	0.54	0.77	0.75	0.76	0.81	0.86	0.51	0.53	0.55	0.52	0.46
Dy	4.96	4.56	4.22	4.86	3.15	4.42	4.33	4.48	4.78	5.22	2.99	2.97	3.22	3.07	2.65
Ho	1.02	0.96	0.86	1	0.66	0.89	0.90	0.90	0.97	1.08	0.59	0.56	0.63	0.63	0.51
Er	2.89	2.76	2.42	2.86	1.91	2.56	2.61	2.51	2.89	3.35	1.72	1.59	1.83	1.82	1.47
Tm	0.42	0.4	0.35	0.42	0.28	0.38	0.39	0.36	0.42	0.51	0.25	0.23	0.27	0.27	0.21

Yb	2.77	2.74	2.37	2.82	1.89	2.5	2.63	2.36	2.75	3.63	1.56	1.51	1.72	1.73	1.41
Lu	0.41	0.41	0.36	0.43	0.28	0.36	0.40	0.35	0.39	0.55	0.22	0.23	0.24	0.23	0.2

Table S4 Principal-components analysis results for the rare earth element (REE) ratios. Based on the best coefficients for PC1 (values > 0.80) and PC2 (values > 0.60), we selected (Gd/Yb)n, (La/Yb)n, (La/Lu)n, the light to heavy REE ratio (LREE/HREE), (La/Gd)n, (La/Sm)n, (Gd/Er)n, and La/Er as fingerprints for the sample similarity analysis.

	Initial eigenvalue			Component matrix		
	Total	Percentage of variance (%)	Cumulative (%)	Trace elements	Coefficients of PC1	Coefficients of PC2
1	5.24	47.69%	47.69%	**Sc**	**0.35**	-0.24
2	2.87	26.16%	73.85%	Rb	0.29	-0.35
3	0.95	8.65%	82.50%	Sr	0.20	-0.37
4	0.64	5.83%	88.33%	**Y**	**0.37**	-0.07
5	0.49	4.54%	92.87%	**Zr**	0.31	0.36
6	0.25	2.33%	95.20%	**Nb**	**0.39**	0.12
7	0.23	2.11%	97.30%	Ba	0.32	-0.15
8	0.16	1.51%	98.82%	**Hf**	0.28	0.40
9	0.09	0.85%	99.67%	**Ta**	**0.34**	0.25
10	0.03	0.32%	99.99%	Pb	0.20	-0.15
11	0	0.01%	100.00%	Th	0.01	0.49

Table S5 Principal-components (PC) analysis results for the trace element ratios and for rare earth elements (REE). Based on the best coefficients for PC1 (> 0.80), we selected the Y/REE, Y/Tb, Y/La, and Y/Nd ratios as fingerprints for the sample similarity analysis.

	Initial eigenvalue			Component matrix		
	Total	Percentage of variance (%)	Cumulative (%)	Trace elements	Coefficients of PC1	Coefficients of PC2
1	6.45	43.01%	43.01%	La/Th	-0.14	0.39
2	4.27	28.48%	71.49%	Zr/Hf	0.13	0.30
3	1.79	11.98%	83.46%	Y/Nb	0.06	0.07
4	1.37	9.16%	92.62%	Nb/Ta	0.33	0.05
5	0.50	3.40%	96.02%	Sc/Y	-0.07	0.37
6	0.32	2.16%	98.18%	**Y/REE**	0.38	0.01
7	0.09	0.63%	98.80%	Th/Sc	-0.01	-0.39
8	0.07	0.51%	99.31%	Th/REE	0.10	-0.44
9	0.04	0.31%	99.62%	**Y/Yb**	0.37	0.05
10	0.03	0.23%	99.85%	**Y/Tb**	0.38	0.02
11	0.01	0.09%	99.94%	**Y/La**	0.38	0.05
12	0	0.04%	99.98%	**Y/Nd**	0.38	0.04
13	0	0.01%	99.99%	Sc/La	0.28	0.22
14	0	0.01%	100.00%	Th/Tb	0.09	-0.44
15	0	0.00%	100.00%	La/Tb	-0.04	-0.02

Table S6 Principal-components analysis results for the rare earth element (REE) ratios. Based on the best coefficients for PC1 (values > 0.80) and PC2 (values > 0.60), we selected (Gd/Yb)n, (La/Yb)n, (La/Lu)n, the light to heavy REE ratio (LREE/HREE), (La/Gd)n, (La/Sm)n, (Gd/Er)n, and La/Er as fingerprints for the sample similarity analysis.

	Initial eigenvalue			Component matrix		
	Total	Percentage of Variance (%)	Cumulative (%)	REE elements	Coefficients of PC1	Coefficients of PC2
1	12.88	92.03%	92.03%	**La**	0.24	0.47
2	0.83	5.94%	97.96%	**Ce**	0.25	0.41
3	0.15	1.14%	99.11%	**Pr**	0.26	0.35
4	0.05	0.38%	99.49%	**Nd**	0.26	0.28
5	0.04	0.34%	99.83%	Sm	0.27	0.15
6	0.01	0.07%	99.90%	Eu	0.26	-0.04
7	0	0.04%	99.94%	Gd	0.27	-0.003
8	0	0.03%	99.97%	Tb	0.27	-0.08
9	0	0.02%	99.98%	Dy	0.27	-0.20
10	0	0.01%	99.99%	Ho	0.27	-0.24
11	0	0.00%	99.99%	Er	0.26	-0.26
12	0	0.00%	100.00%	Tm	0.26	-0.27
13	0	0.00%	100.00%	Yb	0.26	-0.25
14	0	0.00%	100.00%	Lu	0.26	-0.23

Table S7 Principal-components analysis results for the rare earth element (REE) ratios. Based on the best coefficients for PC1 (values > 0.80) and PC2 (values > 0.60), we selected (Gd/Yb)n, (La/Yb)n, (La/Lu)n, the light to heavy REE ratio (LREE/HREE), (La/Gd)n, (La/Sm)n, (Gd/Er)n, and La/Er as fingerprints for the sample similarity analysis.

	Initial eigenvalue			Component matrix		
	Total	Percentage of Variance (%)	Cumulative (%)	REE elements	Coefficients of PC1	Coefficients of PC2
1	6.64	55.38%	55.38%	Eu/Eu*	-0.20	0.21
2	1.84	15.36%	70.74%	δCe	-0.09	-0.34
3	1.57	13.08%	83.82%	(Gd/Yb)n	0.28	-0.34
4	0.90	7.57%	91.40%	**(La/Yb)n**	0.37	0.01
5	0.77	6.43%	97.83%	**(La/Sm)n**	0.27	0.46
6	0.14	1.21%	99.03%	**(La/Lu)n**	0.37	0.03
7	0.07	0.60%	99.63%	**LREE/HREE**	0.35	-0.01
8	0.03	0.31%	99.94%	**(La/Gd)n**	0.05	0.39
9	0	0.03%	99.97%	**(Gd/Er)n**	0.30	-0.37
10	0	0.02%	99.99%	**La/Er**	0.37	0.02
11	0	0.01%	100.00%	Eu/Sm	-0.23	0.23
12	0	0.00%	100.00%	Nd/Sm	0.28	0.37

Figure S1 (a) Spatial distribution of the sample sites shown in Table 1, sample names used at each site, and locations of the weather stations. Site abbreviations: A, Alxa Plateau; C; Hexi Corridor Desert; G, Guerbantonggute Desert; H, Heihe River Basin; L, Lanzhou; M, Mu Us Desert; Q, Qaidam Basin Desert; T, Tengger Desert. (b) Atmospheric dust sampler used in this study.

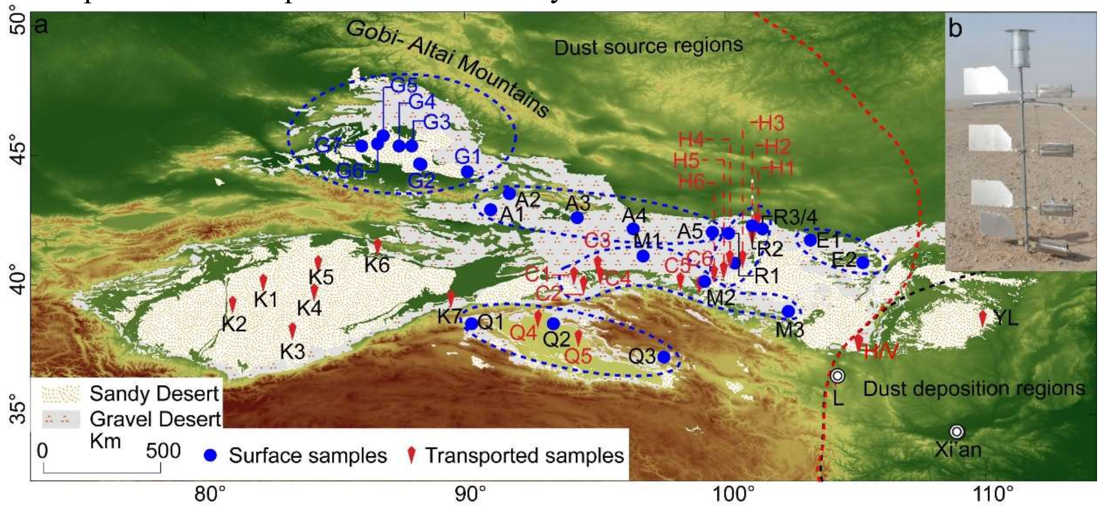

Supplemental References

Bird, A., Stevens, T. , Rittner, M., et al., 2015. Quaternary dust source variation across the Chinese Loess Plateau. Palaeogeogr. Palaeoclimatol. Palaeoecol., 435, 254–264.

Chen, J., Li, G., Yang, J., Rao, J., Lu, H., Balsam, W., Sun, Y., Ji, J., 2007. Nd and Sr isotopic characteristics of Chinese deserts: implications for the provenances of Asian dust. Geochimica et Cosmochimica Acta, 71, 3904–3914.

Chen, X.L., Song, Y.G., Li, J.C., et al., 2017. Size-differentiated REE characteristics and environmental significance of aeolian sediments in the Ili Basin of Xinjiang, NW China. Journal of Asian Earth Sciences, 143, 30–38.

Dong, Z.B., Ping Lv, Zhengcai Zhang, Junfeng Lu. Aeolian transport over a developing transverse dune. Journal of Arid Land, 2014, 6(3): 243–254.

Ding, Z.L., Sun, J.M., Yang, S.L., et al., 2001. Geochemistry of the Pliocene red clay formation in the Chinese Loess Plateau and implications for its origin, source provenance and paleoclimate change. Geochimica et Cosmochimica Acta, 65, 901–913.

Ferrat, M., Weiss, D.J., Strekopytov, S., Dong, S.F., Chen, H.Y., Najorka, J., Sun, Y.B., Gupta, S., Tada, R., Sinha, R., 2011. Improved provenance tracing of Asian dust sources using rare earth elements and selected trace elements for palaeomonsoon studies on the eastern Tibetan Plateau. Geochimica et Cosmochimica Acta, 75, 6374–6399.

Fryberger, S.G., Dean, G., 1979. Dune forms and winds regime. McKee E D. A study of global sand seas. U.S. Geological Survey. US Washington: Geological Survey Professional Paper, 137–169.

Gallet, S., Jahn, B., Torii, M., 1996. Geochemical characterization of the Luochuan loess-paleosol sequence, China, and paleoclimatic implications Chemical Geology,

133, 67–88.
Jahn, B.M., Gallet, S., Han, J.M., 2001. Geochemistry of the Xining, Xifeng and Jixian sections, Loess Plateau of China: eolian dust provenance and paleosol evolution during the last 140 ka. Chemical Geology 178, 71–94.
Kapp, P., Pelletier, J.D., Rohrmann, A., et al., 2011, Wind erosion in the Qaidam basin, central Asia: Implications for tectonics, paleoclimate, and the source of the Loess plateau: GSA Today, 21(4), 4–10.
Licht, A., Pullen, A., Kapp, P., et al., 2016. Aeolian cannibalism: reworked loess as the main sediment source of the Chinese Loess Plateau. GSA Bull, 128, 944–956.
Liu, C.Q., Masuda, A., Okada, A., Yabuki, S., Zhang, J., Fan, Z.L., 1993. A geochemical study of loess and desert sand in northern China: Implications for continental crust weathering and composition. Chem. Geol. 106, 359–374.
Liu, C.Q., Masuda, A., Okada, A., et al., 1994. Isotope geochemistry of Quaternary deposits from the arid lands in northern China. Earth and Planetary Science Letters, 127, 25–38.
Liu, Q.Q., Yang, X.P., 2018. Geochemical composition and provenance of aeolian sands in the Ordos Deserts, northern China. Geomorphology, 318, 354-374.
Maher, B.A., Mutch, T.J., Cunningham, D., 2009. Magnetic and geochemical characteristics of Gobi Desert surface sediments: Implications for provenance of the Chinese Loess Plateau. Geology, 37(3), 279–282.
Rittner, M., Vermeesch, P., Carter, A., Bird, A., Stevens, T., Garzanti, E., Andò, S., Vezzoli, G., Dutt, R., Xu, Z.W., Lu, H.Y., 2016. The provenance of Taklamakan desert sand. Earth and Planetary Science Letters, 437, 127–13.
Stevens, T., Carter, A., Watson, T.P., Vermeesch, P., Andò, S., Bird, A., Lu, H.Y., Garzanti, E., Cottam, M.A., Sevastjanova, I., 2013. Genetic linkage between the Yellow River, the Mu Us desert and the Chinese Loess Plateau. Earth-Sci. Rev. 78(15), 355–368.
Sun, J.M., 2002, Provenance of loess material and formation of loess deposits on the Chinese Loess Plateau. Earth and Planetary Science Letters, 203, 845–859.
Sun, J.M., Ding, Z.L., Xia, X.P., et al., 2018. Detrital zircon evidence for the ternary sources of the Chinese Loess Plateau. Journal of Asian Earth Science, 155, 21–34.
Wei, T., Dong, Z.W., Kang, S.C.,Qin, X., Guo, Z., 2017. Geochemical evidence for sources of surface dust deposited on the Laohugou glacier, Qilian Mountains. Appllied Geochemical, 79, 1-8.
Xie, Y.Y., Chi, Y.P., 2016. Geochemical investigation of dry- and wet-deposited dust during the same dust-storm event in Harbin, China: Constraint on provenance and implications for formation of aeolian loess. Journal of Asian Earth Science, 120, 43-61.
Yang, X., Liu, Y., Li, C., et al., 2007. Rare earth elements of aeolian deposits in Northern China and their implications for determining the provenance of dust storms in Beijing. Geomorphology, 87, 365–377.
Zhang, Z.C., Dong, Z.B., Li, C.X., 2015. Wind regime and sand transport in China's Badain Jaran Desert. Aeolian Res., 17, 1–13.